Don't always blame the photons: relationships between deprotection blur, LER and shot noise in EUV photoresists.

Christopher N. Anderson*

Applied Science & Technology Graduate Group,

University of California at Berkeley, Berkeley, CA 94720, USA

Patrick P. Naulleau

Center for X-ray Optics, Lawrence Berkeley National Laboratory,

1 Cyclotron Road, Berkeley, CA 94720, USA

Abstract

A corner rounding metric has been used to determine the deprotection blur of Rohm and Haas XP 5435, XP 5271, and XP 5496 extreme ultraviolet (EUV) photoresists as base weight percent is varied; an experimental open platform photoresist (EH27) as base weight percent is varied; and TOK EUVR P1123 and FUJI 1195 photoresists as post-exposure bake (PEB) temperature is varied. In the XP 5435, XP 5271, XP 5496, and EH27 resist platforms, a 6 times increase in base weight percent reduces the size of successfully patterned 1:1 lines by over 10 nm and lowers intrinsic line-edge roughness (LER) by over 2.5 nm without changing deprotection blur. In TOK EUVR P1123 photoresist, lowering the PEB temperature from 100 °C to 80 °C reduces measured deprotection blur (using the corner metric) from 30 nm to 20 nm and reduces the LER of 50 nm 1:1 lines from 4.8 nm to 4.3 nm. These data are used to drive a lengthy discussion about the relationships between deprotection blur, LER, and shot noise in EUV photoresists. We provide two separate conclusions: 1) shot noise is probably not the dominant mechanism causing the 3-4 nm EUV LER floor that has been observed over the past several years; 2) chemical contrast contributes to LER whenever deprotection blur is large relative to the printed half pitch.

PACS numbers:

This work was supported by the Director, Office of Science, Office of Basic Energy Sciences, of the U.S. Department of Energy under contract No. DE-AC02-05CH11231.

*Electronic address: cnanderson@berkeley.edu

I. INTRODUCTION

Despite significant progress in the development and optimization of chemically amplified photoresists for extreme ultraviolet (EUV) lithography, current platforms have not simultaneously met the resolution, sensitivity and line-width roughness (LWR) requirements for the 32 nm manufacturing node. Recent work has shown that surface conditioner rinses can be used to smooth LWR and line-edge roughness (LER) in EUV resists by almost one nm with only one nm reduction in critical dimension (CD) [1]. In addition, reduced post-exposure bake (PEB) temperatures have been shown to reduce LER/LWR in sub 50 nm features with modest tradeoffs of reduced photospeed [1]. While LWR is certainly a critical aspect of resists, resolution (or deprotection blur) is arguably even more important due to the fact that it fundamentally limits the patterning ability of dense features.

Several authors have observed that patterning ability in EUV resist improves as base weight percent is increased [2–4]. A contact-hole blur metric [2, 5] was recently used to monitor the blur of several leading EUV photoresists through base and the results indicated that it is unlikely that reduced deprotection blur is the mechanism behind improved patterning ability with increased base loading [6]. At the time of the study, the contact-hole blur metric was chosen over the corner rounding [1, 7, 8] and modulation transfer function (MTF) [9, 10] blur metrics owing to its advantages in terms of reproducibility and robustness in practice [11]. Recent advances in the the measurement of corner rounding [12], however, have also made the corner metric an attractive candidate for deprotection blur measurements.

In this report we use the corner rounding metric to measure the deprotection blur of four resist platforms as base weight percent is varied and two resist platforms as PEB temperature is varied. When possible, the blurs determined here (using the corner metric) are compared to published blurs determined by the contact-hole metric [2, 6]. In addition, we include the LER of 50 nm and 100 nm half-pitch 1:1 line-space patterns for each tested resist/process configuration. This serves to monitor the difference between patterned LER (which measures the LER of features close to the resolution limit of the resist) and intrinsic LER (which measures LER in a regime where the feature pitch is significantly larger than the deprotection blur) as base weight percent and PEB temperature are varied.

II. THE CORNER ROUNDING DEPROTECTION BLUR METRIC

The corner rounding metric has been described in detail in the literature [7] and is based on the measurement of the imaging fidelity of a sharp corner on a large feature. To motivate this point, Figure 1 shows scanning electron microscope (SEM) images of 700 nm dark field elbows printed in Rohm and Haas XP 5496-I and TOK EUVR P1123 photoresists. The sharper corners patterned with the TOK resist are indicative of its overall good performance. In addition, resist models based on the HOST point-spread function (PSF) deprotection blur have shown that the sharpness of printed corners is a good indicator of resist deprotection blur [7].

The corner metric is very straightforward to implement: SEM images of corners of large features (usually from a large-pitch elbow pattern) are captured and analyzed to determine the radius of curvature of each printed corner. The measured radii of several identically coded features are generally averaged to mitigate error sources from mask imperfections and measurement uncertainty in the corner measurement software [12]. Experimental data is then compared to modeling data generated using the HOST PSF resist blur model and the programmed deprotection blur is varied until the modeled printed corner radius matches the experimental data. Once the model data has been generated for a full range of deprotection blurs, the blur extraction step is simply a table look-up provided that mask and illumination conditions match those used for modeling.

As with most PSF-based resolution metrics, the corner metric requires the ability to accurately model the aerial images that create the experimental patterning data. In practice, uncertainties in exposure tool aberrations and focus place constraints on the accuracy to which this can be done. The sensitivity of the corner metric to limitations in aerial image modeling has been previously characterized at the SEMATECH Berkeley MET printing facility [14] assuming 0.15 nm RMS errors in interferometrically measured aberrations [15] and assuming 50 nm focus steps in the FEM. The aerial-image-limited error bars in extracted deprotection blur for the corner metric have been reported at 1.04 nm RMS [7].

III. EXPERIMENT AND RESULTS

A. Resists

We have tested: TOK EUVR P1123 and FUJI 1195 photoresists while varying PEB temperature; three through-base resist series provided by Rohm and Haas based on the XP 5435, XP 5271, and XP 5496 resist platforms; and an experimental open platform through-base series (EH27) provided by the University at Albany [16].

Table I summarizes the resist thickness, post-application bake (PAB), post-exposure bake (PEB), and development parameters for each resist; all process parameters were recommended by the resist supplier [24]. The capital letters next to the Rohm and Haas resists are used to label the relative base weight percents of 0.3, 0.5, 1.0, and 2.0 in the through-base platforms; XP 5435 has an additional base level of 4.0 (XP 5435-H) [25]. The capital letters next to the EH27 resist are used to label the relative base weight percents of 0.33, 0.67, 1.0, 1.5, and 2.0. Four-inch HMDS-primed wafers were used for all experiments and all wafers were developed using a single puddle of Rohm and Haas MF26A.

B. Exposures

All exposures were performed at the 0.3 numerical aperture SEMATECH Berkeley microfield exposure tool printing facility at the Advanced Light Source at Lawrence Berkeley National Laboratory using conventional $\sigma = 0.35 - 0.55$ annular illumination [14] and the LBNL 5,2 dark field mask. Corner features used for the resolution metric are from 700-nm dark field elbow patterns (see Figure 1a) and we use corners with 270 degrees of resist remaining after development.

C. Metrology

All SEM analysis was performed at LBNL on a Hitachi S-4800 with a working distance of 2 mm and an acceleration voltage of 2.0 kV. All line-space and corner data were characterized using offline analysis software [12]. Corner radius values are determined with the removed area method [7] and the values used for blur extraction are the average of the 7 corners in the elbow pattern shown in Figure 1a. LER data for line-space patterning is obtained using

a 3x3 dose-focus process window around the center-dose center-focus site in the FEM. For 100 nm 1:1 features the SEM magnification is set to 100k providing 6 patterned lines in each SEM image. The reported LER magnitude is the average of the 54 single-line LER values in the process window and the reported LER uncertainty is the 3σ standard deviation of the 54 single-line LER values divided by the square root of the number of lines in the process window. For 50 nm features the SEM magnification is set to 150k providing 8 patterned lines per SEM image and 72 lines in the process window. The spatial frequency spectrum of a single-line LER measurement is confined to a passband with a minimum period of 10 nm (just above the noise floor) and a maximum period of 834 nm (the height of the SEM image). Correlation length numbers are computed using the height-height correlation function (HHCF) method [18]. The patterning limit is defined as the smallest sized 1:1 lines that pattern in resist without excessive collapse or fusing. E-size is the dose required to print 50 nm 1:1 features at their coded size at best focus; we use the new dose calibration adopted at SPIE 2008 [17].

D. Results

Table II summarizes various performance metrics for all tested resist and process formulations. The new corner method deprotection blur data is alongside published blur data determined with the contact method for comparison purposes [6]. The deprotection blurs for Rohm and Haas XP 5435-F and FUJI 1195 were never determined using the contact method and as a result this data is missing from the table.

IV. DISCUSSION

A. Deprotection blur metrics

On average, the extracted blurs for the corner metric are higher than the contact metric, with this being the most prevalent in the EH27 and EUVR P1123 platforms. Experimentally, the EH27 and XP 5435 platforms pattern similarly through base and one would expect that their deprotection blurs are close in magnitude; the blur of EH27 determined with the corner method agrees more with direct observation. The discrepancy between the contact and corner metric blur numbers may stem from subtle differences in resist performance when

pattering 50-nm contacts vs. 700-nm corners; however both features are based off of a structure with 270 degrees of resist and 90 degrees of removed resist so it is not straightforward to argue why one might perform better than the other.

The strength of the corner and contact metrics is really the ability to track diffusion blur in resists while perturbing resist and process parameters. In terms of serving this purpose, the contact and corner metrics have both shown remarkable precision in practice. Although the blur numbers do not agree in an absolute sense in all platforms, both metrics show the same deprotection blur trends as process parameters are varied within a resist platform. Since both metrics require less than ten SEM images and are relatively low overhead in terms of modeling support, they can be used in parallel in situations where one or the other might yield inconclusive results.

B. The relationship between deprotection blur and patterned LER

It is generally assumed that LER can be improved by increasing the deprotection blur. Fundamental to this assumption is that the "pixel size" relevant for counting statistics is determined by the average size of the diffusion or blur sphere. The resulting conclusion is that larger resist blurs lead to bigger counting bins, more absorbed photons per bin, better counting statistics, and reduced LER. However, Steenwinckel et. al. [3] has reported that as the acid diffusion length becomes large relative to the size of the feature being patterned, the LER reduction from improved counting statistics becomes dominated by an increase in LER due to reduced chemical contrast. Several examples from these data defend this interpretation and reaffirm that deprotection blur can be a significant contributor to patterned LER:

1. The aerial image log slope for 50 nm and 100 nm line-space features is similar owing to their large size relative to the diffraction limit of the optic [15]. However, patterned LER is larger than intrinsic LER in every resist we tested where the deprotection blur is larger than 30 % of the half pitch (five out of six resists).

2. In the P1123 PEB temperature experiment, increasing the deprotection blur by 20 % of the half pitch increases patterned LER by 12 % and leaves intrinsic LER unaffected.

3. At E-size ≈ 7 mJ/cm^2 (the only value common to every tested platform) the fractional difference between patterned and intrinsic LER is largest in the high blur platforms (5435 and 5271) and smallest in the low blur platforms (1195 and 1123).

C. The intrinsic LER floor

Looking at these data in total, it is clear that the intrinsic LER seems to level off at about 4 nm. Of course, this is nothing new. There have been several publications that show EUV intrinsic LER leveling off at $\approx$ 3-4 nm across a wide range of resists [20]. The mechanisms that cause the EUV intrinsic LER floor are not well understood at the present time. There are two experiments known to the authors in which LER is measured as base weight percent is changed in an EUV resist [3, 4]. In both of these experiments their authors claim that improvements in LER with increased base weight percent are directly correlated with reductions in shot noise.

In discussions related to EUV LER it is very important to make the distinction between two things: the signal to noise ratio (SNR) [26] of absorbed photons (related to shot noise) and the SNR of photo-generated acids; the two are not necessarily the same. In deep ultraviolet (DUV) ($\lambda = 248$ nm) exposures, photons are primarily absorbed by photo acid generator (PAG) molecules [16]. As a result, an absorbed photon really is the same as a photo-generated acid. The situation is very similar with 193 nm light. At EUV wavelengths the creation of acid is an entirely different mechanism. As described in detail by Brainard et. al. [16], the general picture is that an EUV photon ionizes a polymer monomer and subsequently creates a cascade of secondary electrons each capable of producing an acid. If an electron finds a PAG, an acid is generated. While this distinction between EUV and DUV exposures is subtle, it is very important. The reason it is important is because LER is ultimately influenced by the SNR of acids, not the SNR of absorbed photons. To drive this point home, consider two different exposure scenarios where an average of N PAG molecules are activated per pixel.

1. N $\ll$ the average number of PAG molecules per pixel.

2. N $\approx$ the average number of PAG molecules per pixel.

In scenario 1, increasing the dose will cause more photons to be absorbed by the resist

film. As a result, the SNR of absorbed photons will increase through Poisson statistics (a reduction in shot noise). Due to the high availability of non-activated PAGs, the increase in absorbed photons will translate almost directly to an increase in photo-generated acids. Consequently, the SNR of acids will increase if Poisson statistics are assumed. In this scenario, it follows that the SNR of acid is limited by the availability of photons, not the distribution of PAG molecules.

In scenario 2, increasing the dose will again cause more photons to be absorbed by the resist film. And again, the SNR of absorbed photons will increase through Poisson statistics (again, shot noise is reduced). However, since there are no more available PAG molecules, the increase in absorbed photons cannot translate to an increase in photo-generated acid. Consequently the SNR of acid does not improve by increasing the dose. In this scenario the SNR of acid is not limited by the availability of photons; it is limited by the distribution statistics of the PAG molecules.

Increasing the amount of base in a resist always shifts the exposure conditions more towards scenario 2. The reason for the shift is that adding base requires a higher concentration of photo-generated acid to achieve the same amount of deprotection. As a result, a larger fraction of available PAG molecules must be activated during exposure whenever base is increased. If base and dose scaling are used to reduce intrinsic LER, eventually the fraction of activated PAG molecules becomes large enough that the PAG distribution plays a role in determining the SNR of photo-generated acid. If this is continued, the SNR of photo-generated acids is ultimately limited by the distribution statistics of PAG molecules.

It is difficult to know for sure whether or not we have seen acid SNR's that are significantly effected by the PAG distribution. However, in three of the four through base resist series' we have tested (5435, 5271 and 5496) the drop in LER in going from the second highest base weight percent to the highest weight percent is at least a factor of two less than expected form the square root of the relative change in E-size. This indicates that in these three resists, the exposure regime is somewhere between scenarios 1 and 2 where the PAG distribution does affect the SNR of photo-generated acids. While there is no conclusive evidence that the PAG distribution is fully responsible the intrinsic LER floor, we believe these data suggest that it is unlikely that shot noise is the sole / dominant contributor. Many other factors may also influence fundamental LER limits. Some that the authors are aware of are: developer percolation [21], mesoscale resist properties [22], and local variations in critical ionization

and dissolution properties [23].

Finally, we would like to point out that while it is believed that larger deprotection blurs equate to larger counting bins and improved overall statistics, we observe no obvious correlation between higher deprotection blur and lower intrinsic LER.

V. SUMMARY

Shot noise is probably not the dominant mechanism causing the 3-4 nm EUV LER floor that has been observed over the past several years [20]. In three resists with LERs approaching the LER floor, the LER drop associated with scaling up base and dose is at least a factor of two less than expected from shot noise arguments. We speculate that it is possible these trends are due to the PAG distribution playing a role in fundamental LER limits. While it is often assumed that larger deprotection blurs improve intrinsic LER by scaling counting statistics through larger counting bins, we have seen no evidence of this effect in our data. Finally, we have confirmed that chemical contrast contributes to LER whenever deprotection blur is large relative to the printed half pitch.

VI. ACKNOWLEDGMENTS

The authors are greatly indebted to Paul Denham, Brian Hoef, Gideon Jones, Jerrin Chiu, and Ken Goldberg of the Center for X-Ray Optics at Lawrence Berkeley National Laboratory for expert support with the exposure tool as well as the entire CXRO engineering team for building and maintaining the EUV exposure tool. The authors also acknowledge Jim Thackeray and Katherine Spear from Rohm and Haas, Koki Tamura, Chris Rosenthal, and Dave White from TOK, and Shinji Tarutani from Fujifilm for supplying resist and process support. In addition, the authors acknowledge Robert Brainard from the University at Albany for resist support and valuable discussions related to this work. The authors are grateful for support from the NSF EUV Engineering Research Center. This research was performed at Lawrence Berkeley National Laboratory using the SEMATECH-supported MET exposure facility at the Advanced Light Source. Lawrence Berkeley National Laboratory is operated under the auspices of the Director, Office of Science, Office of Basic Energy Science, of the

US Department of Energy.

---

[1] T. Wallow, R. Kim, B. La Fontaine, P. Naulleau, C. Anderson, R. Sandberg, "Progress in EUV Photoresist Technology," Proc SPIE 6533, 653317 (2007)

[2] C. Anderson, P. Naulleau, D. Naikoula, E. Hassanien, R. Brainard, G. Gallatin, K. Dean, "Influence of base and PAG on deprotection blur in EUV photoresists and some thoughts on shot noise," JVST B 26 (6) Nov/Dec 2295-2299 (2008).

[3] D. Steenwinckel, J. Lammers, T. Koehler, R. Brainard, and P. Trefonas, "Resist effects at small pitches," JVST B 24 (1) Jan/Feb 316-320 (2006).

[4] R. Brainard, P. Trefonas, J. Lammers, C. Cutler, J. Mackevich, A. Trefonas, and S. Robertson, "Shot noise, LER and quantum efficiency of EUV photoresists," Proc. SPIE 5374 74-85 (2004).

[5] P. Dirsken, J. Braat, A. J.E.M. Janssen, A. Leeuwestein, H. Kwinten, and D. V. Steenwinckel, "Determination of resist parameters using the extended Nijboer-Zernike theory," Proc. of SPIE 5377 150-159 (2004).

[6] C. Anderson and P. Naulleau, "Deprotection blur in extreme ultraviolet photoresists: influence of base loading and post-exposure bake temperature," Accepted JVST B Jan/Feb 2009 (MS # 37486).

[7] C. Anderson and P. Naulleau, "Sensitivity study of two high-throughput resolution metrics for photoresists," Appl. Opt. Vol 47, No. 1 56-63 (2008).

[8] P. Naulleau and C. Anderson "Lithographic metrics for the determination of intrinsic resolution limits in EUV resists," Proc. SPIE 6517 65172N (2007)

[9] J. Hoffnagle, W. D. Hinsberg, F. A. Houle, and M. I. Sanchez, "Characterization of photoresist spatial resolution by interferometric lithography", Proc. SPIE 5038, 464-472 (2003).

[10] T. Brunner, C. Fonseca, N. Seong, M. Burkhardt, "Impact of resist blur on MEF, OPC and PD control," Proc. SPIE 5377 141-149 (2004)

[11] C. Anderson and P. Naulleau, "A high-throughput contact-hole resolution metric for photoresists: full-process sensitivity study," Proc. SPIE 6923 69230Z (2008).

[12] SuMMIT software is distributed by EUV Technology, Martinez, CA 94553, http://www.euvl.com/summit

[13] C. Ahn, H. Kim, and K. Baik, "A novel approximate model for resist process," Proc. SPIE

3334, 752763 (1998).

[14] P. Naulleau "Status of EUV micro-exposure capabilities at the ALS using the 0.3-NA MET optic," Proc. SPIE 5374, 881-891 (2004).

[15] K. Goldberg, P. Naulleau, P. Denham, S. Rekawa, K. Jackson, E. Anderson, and J. Alexander Liddle. "At-Wavelength Alignment and Testing of the 0.3 NA MET Optic, J. Vac. Sci. and Technol. B 22, 2956-2961 (2004).

[16] R. Brainard, E. Hassanein, J. Li, P. Pathak, B. Thiel, F. Cerrina, R. Moore, M. Rodriguez, B. Yakshinskiy, E. Loginova, T. Madey, R. Matyi, M. Malloy, A. Rudack, P. Naulleau, A. Wuest, K. Dean, "Photons, electrons and acid yields in EUV photoresists: a progress report," Proc. SPIE 6923 692325 (2008)

[17] P. Naulleau, E. Gullikson, A. Aquila, S. George, D. Niakoula, "Absolute sensitivity calibration of extreme ultraviolet photoresists, Opt. Exp. 16, 11519-11524 (2008).

[18] V. Constantoudis, G. Patsis, A. Tseperi, E. Gogolides, "Quantification of line-edge roughness of photoresists. II. Scaling of fractal analysis and and the best roughness descriptors," JVST B 21(3) May/Jun 1019-1026 (2003).

[19] P. Naulleau and G. Gallatin, "Spatial scaling metrics of mask-induced line-edge roughness," JVST B 26(6) Nov/Dec 1903-1910 (2008).

[20] P. Naulleau, C. Anderson, J. Chiu, K. Dean, P. Denham, S. George, K. Goldberg, B. Hoef, G. Jones, C. Koh, B. La Fontaine, A. Ma, W. Montgomery, D. Niakoula, J. Park, Tom Wallow, Stefan Wurm, Latest results from the SEMATECH Berkeley extreme ultraviolet microfield exposure tool, JVST B 26(6) Nov/Dec (2008).

[21] H. Fukuda and A. Yamaguchi, "LER as structural fluctuation of resist reaction and developer percolation," Proc. of SPIE 4691 158-168 (2002).

[22] J. Meiring, T. Michaelson, A. Jamieson, G. Schmid, C. Willson, "Using mesoscale simulation to explore photoresist line edge roughness," Proc. SPIE, Vol. 5753, 350-355 (2005).

[23] V. Sarris, G. P. Patsis, V. Constantoudis, A. G. Boudouvis1 and E. Gogolides, "A stochastic photoresist-polymer dissolution model combining the percolation and critical ionization models," Jpn. J. Appl. Phys. 44 7400-7403 (2005).

[24] FUJI 1195 and TOK EUVR P1123 have supplier-recommended PEB temperatures of 90 °C and 100 °C, respectively

[25] The letter J corresponds to base weight percents of 2.0 and 0.3 in the XP 5496 and XP 5271

platforms, respectively.

[26] The ratio of the average number of events per pixel and the standard deviation of the number of events per pixel where a pixel is a volume of space

List of Figures

List of Tables

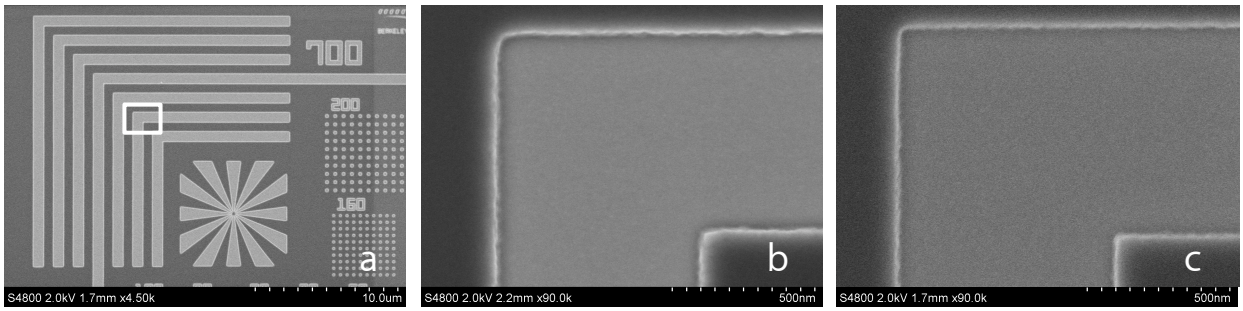

FIG. 1: (a) SEM image of a 700-nm elbow pattern from the LBNL 5,2 dark field mask. The white box shows the zoomed region in subfigures b and c; (b) 700 nm elbow printed in Rohm and Haas XP 5496I photoresist; (c) 700 nm elbow printed in TOK EUVR P1123 photoresists.

TABLE I: Process parameters for tested resist formulations.

Supplier	Resist	Thickness (nm)	PAB (°C)	PAB (sec)	PEB (°C)	PEB (sec)	Dev. time (sec)
Rohm and Haas	XP 5435 E,F,D,G,H	120	130	60	130	90	45
Rohm and Haas	XP 5271 J,K,D	80	130	60	120	90	45
Rohm and Haas	XP 5496 H,I,F,J	80	130	60	90	90	45
Rohm and Haas	XP 4502 D	120	130	60	120	90	45
University at Albany	EH27 C,D,E,F,G	125	130	60	130	90	45
TOK	EUVR P1123	60	120	60	80, 90, 100	90	60
FUJI	1195	80	120	90	90, 100, 110	90	30

TABLE II: EUV resist performance metrics

Resist	Base % (relative)	Blur (nm) *Contact*	Blur (nm) *Corner*	Pattern limit (nm 1:1)	LER (nm) 50 nm 1:1	LER (nm) 100 nm 1:1	Lc (nm) 50 nm 1:1	Lc (nm) 100 nm 1:1	E-size (mJ/cm^2)
XP 5435-E	0.3	32.1	36.8	52	13.7 ± 0.6	8.2 ± 0.1	39.1	29.9	1.6
XP 5435-F	0.5		38.4	50	8.2 ± 0.4	5.8 ± 0.1	37.1	27.8	2.3
XP 5435-D	1.0	31.3	35.0	42	6.1 ± 0.3	5.7 ± 0.2	35.6	31.2	3.2
XP 5435-G	2.0	26.2	33.8	40	5.5 ± 0.3	4.6 ± 0.1	29.9	37.9	6.4
XP 5435-H	4.0	25.1	30.0	36	5.0 ± 0.3	4.0 ± 0.1	29.9	31.5	14.0
XP 5271-J	0.3	27.9	31.2	47	13.4 ± 0.8	8.0 ± 0.2	25.8	25.2	4.0
XP 5271-K	0.5	25.4	32.3	43	6.7 ± 0.3	5.3 ± 0.1	22.9	37.0	6.5
XP 5271-D	1.0	23.8	34.8	39	6.7 ± 0.2	5.2 ± 0.1	20.6	26.1	12.5
XP 5496-H	0.3	26.5	27.6	48	8.1 ± 0.3	7.6 ± 0.1	22.3	23.5	3.0
XP 5496-I	0.5	26.4	28.1	44	7.9 ± 0.3	6.9 ± 0.1	20.2	23.3	4.7
XP 5496-F	1.0	24.6	27.0	38	6.5 ± 0.3	5.8 ± 0.1	18.9	29.9	7.6
XP 5496-J	2.0	25.0	29.2	38	5.3 ± 0.3	5.0 ± 0.1	22.2	26.9	15.2
EH27-C	0.3	17.0	33.2	52	13.4 ± 0.7	6.9 ± 0.1	25.6	24.4	1.9
EH27-D	0.7	17.3	35.0	47	8.8 ± 0.4	5.8 ± 0.1	28.1	22.1	3.2
EH27-E	1.0	16.7	37.0	43	6.8 ± 0.2	4.9 ± 0.1	29.5	27.1	6.4
EH27-F	1.5	15.0	32.3	42	5.3 ± 0.1	4.9 ± 0.1	23.7	25.0	7.8
EH27-G	2.0	17.1	36.6	39	4.5 ± 0.1	4.1 ± 0.1	27.6	27.1	10.7
P1123 (80° PEB)	1.0	9.7	19.6	28	4.3 ± 0.1	4.0 ± 0.1	18.1	25.1	11.9
P1123 (90° PEB)	1.0	13.5	24.1	28	4.5 ± 0.1	4.0 ± 0.1	15.7	21.7	8.8
P1123 (100° PEB)	1.0	21.1	30.0	30	4.8 ± 0.1	4.1 ± 0.1	17.7	20.2	8.2
1195 (90° PEB)	1.0		18.0	27	3.9 ± 0.1	4.1 ± 0.1	20.1	22.7	9.8
1195 (100° PEB)	1.0		18.0	26	3.7 ± 0.1	3.9 ± 0.1	21.2	27.2	10.4
1195 (110° PEB)	1.0		17.5	26	3.9 ± 0.1	4.1 ± 0.1	29.1	30.1	10.4